Fabrication and Testing of Flexible Pulsating Heat Pipes

Nicholas Morgan, Damian Hundley, Maya Baron, Matthew Pichardo, Shawn A. Putnam Department of Mechanical and Aerospace Engineering University of Central Florida, Orlando, FL 32816

Email: shawn.putnam@ucf.edu

Abstract—The demand for flexible microelectronics has increased significantly within the last decade. This study investigates the cooling performance of flexible pulsating heat pipes (PHPs) made from acrylic with a bend radius of $\approx\!300$ mm. The fabricated devices support two-phase, pulsating fluid flow inside the rectangular microchannels. Both water and ethanol are used as coolants, where local hot spots are generated by cobalt-alloy foil heaters inside the flexible PHPs. The PHP's dissipate the heat generated to the environment via copper condensers with controlled setpoint temperatures. Based on a heater surface area of $\approx\!1.5~\text{cm}^2$ and a condenser setpoint temperature of 25°C , the maximum heat flux observed for sustained and repeatable cooling with water and ethanol was 8 W/cm². These heat fluxes correlate well with other PHP studies with similar heater power loads, channel geometries, and coolants.

I. INTRODUCTION

Passive cooling is important for optimizing the performance of various computational devices. The field of electronics is trending sharply towards the use of flexible devices that are not only lighter in weight but also have low manufacturing costs. Pulsating heat pipes have shown to be a promising candidate due to their higher cooling efficiencies relative to cooling with single-phase fluids [1]. PHPs are also capable of being manufactured out of flexible materials and can contain a variety of microchannel patterns and geometries for a widerange of different applications [1, 2, 3, 4, 5]. Fig. 1 depicts the PHP devices studied herein. Recently there has been increased interests in PHPs for flexible microelectronics. Many studies have investigated copper PHPs due to their high thermal conductivity and capability to dissipate heat fluxes approaching 30 W/cm² [6]. While copper is ductile, copper PHPs are not well suited for flexible electronics. In result, recent advancements with soft polymer PHPs have achieved similar heat fluxes; yet, are flexible with bend radii and thicknesses approaching $\lesssim 10$ mm and $\lesssim 1$ mm, respectively [7].

The PHP cooling performance is dictated by many factors, including channel diameter, channel length, coolant fill ratio, orientation relative to gravity, and the thermophysical properties of the coolant itself [8]. All these parameters influence the oscillation dynamics of the liquid-vapor interfaces (or liquid slugs) inside the PHP. The liquid slugs oscillate primarily in the adiabatic region (between the evaporator and condenser regions) due to natural convection. In addition, most studies use water as a coolant because of water's high heat capacity, high latent heat of vaporization, low cost, and low health

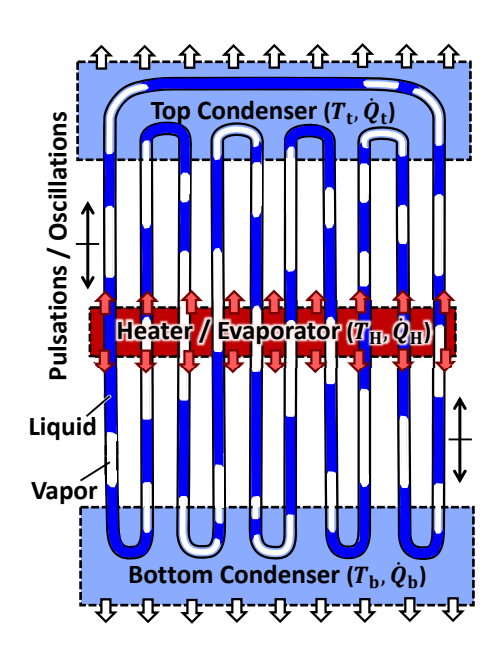


Fig. 1. Schematic depiction of pulsating heat pipe with central heating and dual (top and bottom) condenser regions.

hazards [9, 10]. However, at standard pressures the boiling point of water is near the glass transition (or melting) temperature of most polymers (T_g or T_m); thus, water-polymer-based PHPs are highly likely to warp if overheated. Ethanol, while its thermophysical properties are not as attractive as that of water, ethanol has a standard boiling point below T_g and also yields similar heat flux removal capabilities as water [11]. Other fluids that are well suited for flexible, polymer-based PHPs include refrigerants such as Novec 7000 [5]. Table 1 shows different working fluids and their corresponding thermophysical properties.

The efficiency of any liquid cooling technique is typically quantified in terms of the heat transfer coefficient (h, HTC). The HTC is a proportional relation between the heat flux, q, and the temperature difference ΔT between that of the working fluid and that of the device surface in the evaporator region (Fig. 1). However, aside from the nucleate boiling heat transfer regime, the HTC can vary quite significantly with changes in both q and ΔT . An upper-limit to the HTC is tied to the critical heat flux (CHF), where significant reductions in the HTC (i.e., the cooling efficiency) are observed once

Fluid	Water	Ethanol	FC-72	Novec 7000
Boiling Point (°K)	373.15	351.15	329.26	307.04
h _{fg} (kJ/kg)	2260	864	88	142
c _p (J/kg⋅K)	4.181	2.57	1.014	1.13

the heat flux reaches or surpasses the CHF. Also, if the CHF is exceeded, then the PHP device may experience irreversible damage. Therefore, PHPs typically operate below the CHF within the nucleate boiling regime [12, 13].

II. METHODOLOGY

A. Experimental Setup

The PHP devices studied were designed to account for optimal performance based on the coupling between the channel dimensions, device geometry, and the thermophysical properties of the fluid coolant. Many studies have shown that optimal PHP performance is achieved when the Bond number is less than one [14] (Bo = $\Delta \rho g L_c^2/\sigma < 1$). For example, the maximum hydrodynamic channel radius $(r_{\rm ch,\ max} = L_c)$ can be calculated for Bo ≈ 0.85 [4, 14] using

$$r_{\rm ch, \ max} \le \sqrt{\frac{\sigma {
m Bo}}{g(
ho_{
m L} -
ho_{
m v})}},$$
 (1)

where σ represents the surface tension of the fluid, g is the gravitational acceleration, and ρ is the density of the fluid. PHPs studied in this work had channel diameters of \approx 575 μ m and were fabricated by micro-milling acrylic polymer substrates [15].

Fig. 2 shows an exploded view of the PHP system studied in this work. To simulate the heat produced by microelectronics, cobalt-alloy thin-film heaters were cut to dimensions similar to that depicted in Fig. 2. Based on the geometry of the heater and busbar connections, the area of the heater is

$$A_{\text{heat}} = (L_{\text{heat}} \cdot W_{\text{heat}}) + [(L_{1, \text{bus}} + L_{2, \text{bus}}) \cdot W_{\text{bus}})],$$
 (2)

where L and W are the length and width of the heater (or busbars), respectively. This thin-film, strip heater was placed in the middle of the PHP (Figs. 1-3). Also, a T-type thermocouple was placed near the heater surface in the PHP to gather local temperature data in the evaporator region. To close the system, a circular sapphire (Al₂O₃) window was used because sapphire is transparent in both the visible and Mid-wave IR (MWIR) wavelength spectrum, facilitating both visible imaging and MWIR thermometry characterization during PHP operation. Since sapphire has a high thermal conductivity relative to that of the acrylic polymer PHP walls ($k_{\rm Al_2O_3} \approx 46~{\rm W/m\cdot K}$ at 25°C >> 0.2 W/m·K), the sapphire window induces significant conjugate heat transfer. To minimize the conjugate heat transfer in the sapphire window, a thin-film of perfluoroalkoxy polymer (PFA) was placed in between the

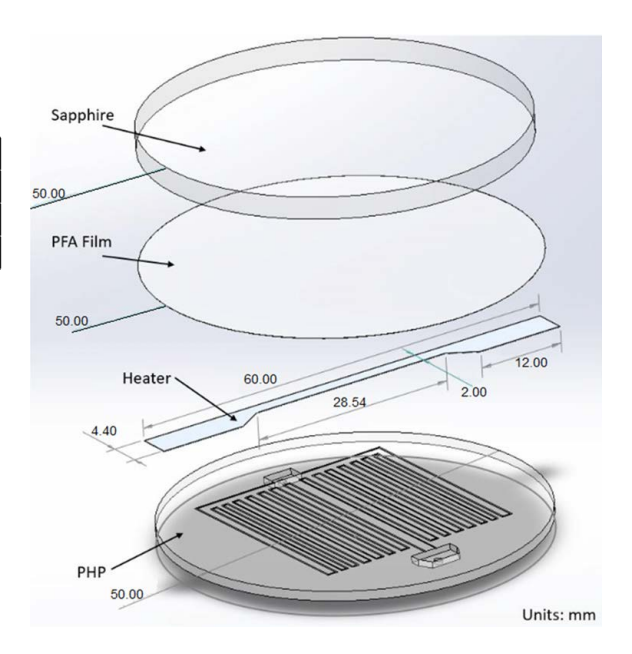


Fig. 2. Exploded view of PHP.

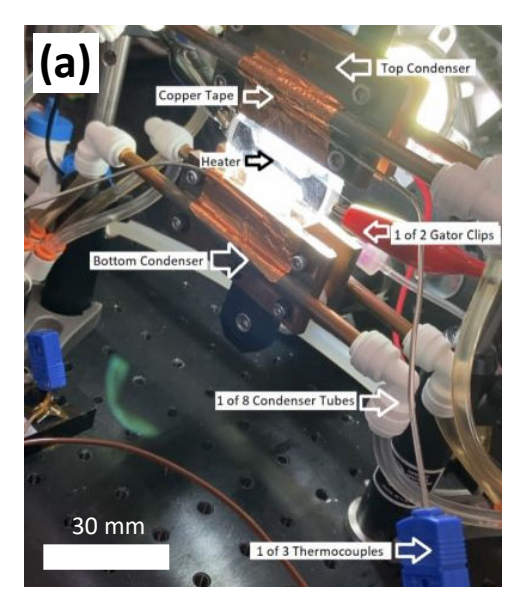
sapphire and the acrylic PHP. The thickness of PFA film was $\approx 25 \mu m$. The PFA thin-film was also MWIR transparent ($\approx 99\%$) and has a thermal conductivity comparable to that of acrylic ($k \approx 0.23$ W/m·K at 25°C). The heater, PFA film, and sapphire were pressure fitted and then sealed using the UV light curable Norland Optical Adhesive (NOA-61). After the NOA-61 was UV-cured, two holes were drilled into the PHP so that fluid could be injected into the microchannels.

Fig. 3 (a) shows an image of the complete testbed. The high intensity light placed behind the PHP device facilitates high-speed videography characterization. The test setup uses two condensers that are temperature regulated at 25°C by an external chiller and cooling lines. The back plates of each condenser (top and bottom) have o-ring sealed fluid through ports for subsequent coolant loading and unloading. Therefore, after assembly and alignment, the PHP is filled to a desired fill ratio by injecting the coolant into the bottom fill port. Then both the fill ports are closed for testing. A programmable variable AC-DC power supply provides AC current to the heater for controlled joule heating thermal loading.

B. IR Camera Setup and Temperature Measurements

The pulsation dynamics (for various AC power loads) are visualized by both high-speed visible videography and MWIR thermography. IR imaging is mainly used to monitor the spatiotemporal device temperatures during an experiment. Fig. 3 (b) provides a snapshot image acquired by the MWIR camera during a PHP experiment. The effective emissivity of the PFA thin-film for IR thermography was ≈ 0.45 .

Temperature data is also acquired from three thermocouples (one near the heater and two others near each condenser) by a Data Acquisition (DAQ) system. Thus, the temperatures inside the PHP are measured by the thermocouples and the IR camera. This helps with not only calculating heat flux and HTC



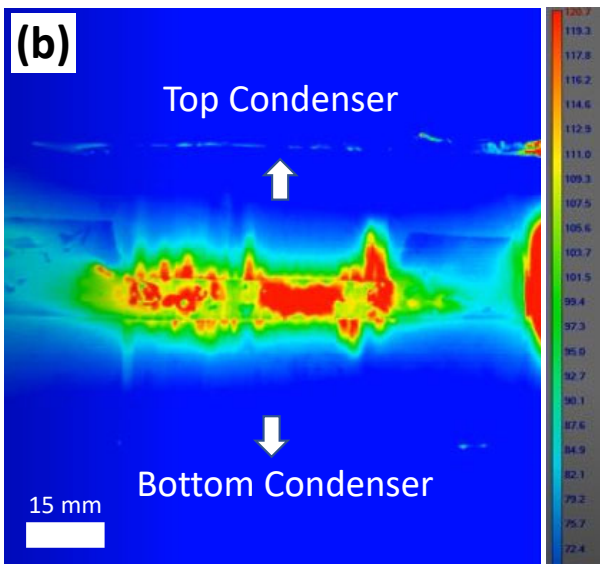


Fig. 3. (a) PHP experimental test-bed. (b) MWIR thermography image of PHP with water at 23 W.

values (especially during steady-state operation), but also helps with plotting the average change in the device temperature in an experiment with comparisons to that acquired by the thermocouples.

C. High-Speed Camera Measurements

Since IR imaging with our MWIR camera setup has its limitations on the spatial and temporal resolutions of the pulsation dynamics, high-speed visible imaging is used in parallel. High-speed visible imaging is mainly used to track the liquid slug locations and pulsation amplitudes as a function of time. Using a python code and computer vision (OpenCV), we can generate a threshold mask for a specified region of interest (ROI) where the liquid slug is pulsating. The code then creates a rectangle around the vapor plug contour and tracks the movement of the vapor plug. Three rectangles are created, a red rectangle tracks a plug with the most movement, a blue rectangle tracks a plug with moderate movements, and a green rectangle tracks a plug with minimal movements. Fig. 4 (a) shows a static image of the original recording and Fig. 4 (b) shows the image after the mask is applied. As the code tracks the movement of the three plugs, it simultaneously plots the amplitudes by finding the difference between the endpoint of the liquid slug and a reference point frame by frame.

D. Heat Transfer Calculations

The heat flux of a pulsating heat pipe is governed by the power input and the surface area of the heater. It can be calculated by the following equation

$$q = \frac{\mathcal{P}_{\text{in}}}{A_{\text{heat}}}.$$
 (3)

 \mathcal{P}_{in} represents the power input to the evaporator region. Using the heat flux, the heat transfer coefficient is calculated by

$$h = \frac{q}{\Lambda T}. (4)$$

Eq. 4 is the general equation for the HTC and is also used by others [13, 8, 14] for the HTC of a PHP.

As the heater increases in temperature, so does the pressure in the evaporator region due to nucleate boiling[13]. Using the Clausius-Clapeyron relation, the evaporator pressure $P_{\rm evap}$ can be expressed as

$$P_{\text{evap}} = P_0 \exp\left[\frac{h_{\text{fg}}(T_{\text{evap}} - T_{\text{cond}})}{\Re(T_{\text{evap}})(T_{\text{cond}})}\right],\tag{5}$$

where $P_0 = \rho_{\rm v} \mathcal{R}(T_{\rm evap} - T_{\rm cond})$ is the reference pressure, $h_{\rm fg}$ is the latent heat of vaporization of the working fluid, \mathcal{R} is the specific gas constant, and $T_{\rm evap}$ and $T_{\rm cond}$ are the evaporator and condenser temperatures respectively. From Eq. 5, the change in pressure ΔP between the evaporator and condenser regions can be found via

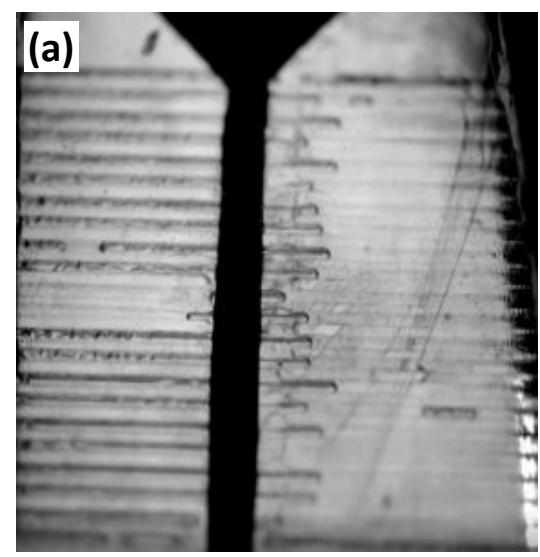
$$\Delta P = P_0(\exp\left[\frac{h_{\rm fg}(T_{\rm evap} - T_{\rm cond})}{\mathcal{R}(T_{\rm evap})(T_{\rm cond})}\right] - 1). \tag{6}$$

After applying a second order Taylor series expansion to Eq. 6, the ΔP simplifies to

$$\Delta P = \Delta T \frac{h_{\rm fg} \rho_{\rm v}}{T_{\rm evap}} \left[1 + \frac{1}{2} \left(\frac{h_{\rm fg} \Delta T \rho_{\rm v}}{P_0 T_{\rm evap}} \right) \right]. \tag{7}$$

When Eq. 7 is plotted as a function of time, ΔP is sinusoidal and decreases in magnitude in time. As vapor is generated in the evaporator region, the pressure inside the microchannels and ΔP a single liquid slug can be expressed as

$$dP_{\text{evap}} = \frac{dP_{\text{evap}}}{d\rho_{\text{v}}} \cdot d\rho_{\text{v}},\tag{8}$$



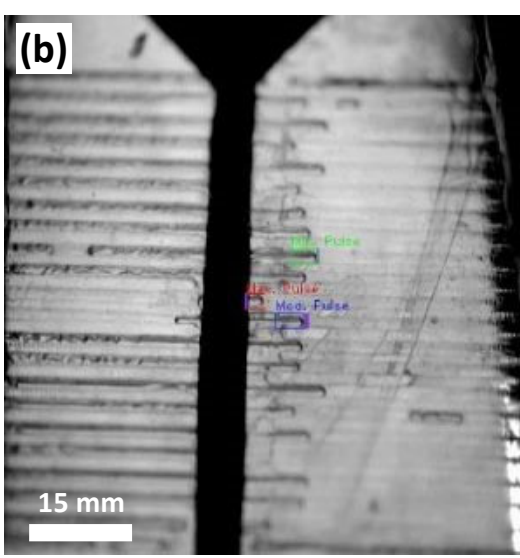


Fig. 4. Images from the high-speed camera that show (a) ethanol liquid slugs and vapor plugs inside of the PHP and (b) the same image after a mask has been applied, tracking the plugs within a specified region of interest (ROI). In (b), the red text reads "Max. Pulse", blue text reads "Mod. Pulse", and the green text reads "Min. Pulse".

where $\rho_{\rm v}$ is the density of the vapor. From Eq. 5, mass conservation can be applied to the vapor, yielding

$$dP_{\text{evap}} = \frac{dP_{\text{evap}}}{d\rho_{\text{v}}} \cdot (-\rho_{\text{v}}) (\frac{A_{\text{c}}}{V_{\text{v}}}) dx, \tag{9}$$

where $A_{\rm c}$ is the cross-sectional area of the fluid in the microchannels, and $V_{\rm v}$ is the volume of the vapor. Using Eq. 6, the gas spring constant κ (which describes the oscillation amplitude based on the forces from the evaporator and condenser regions acting on the fluid) can be expressed as

$$\kappa = \frac{dP_{\text{evap}}}{d\rho_{\text{v}}} \cdot (\rho_{\text{v}}) (\frac{A_{\text{c}}^2}{V_{\text{v}}}). \tag{10}$$

Fig. 5 shows the model of the gas spring constant of the

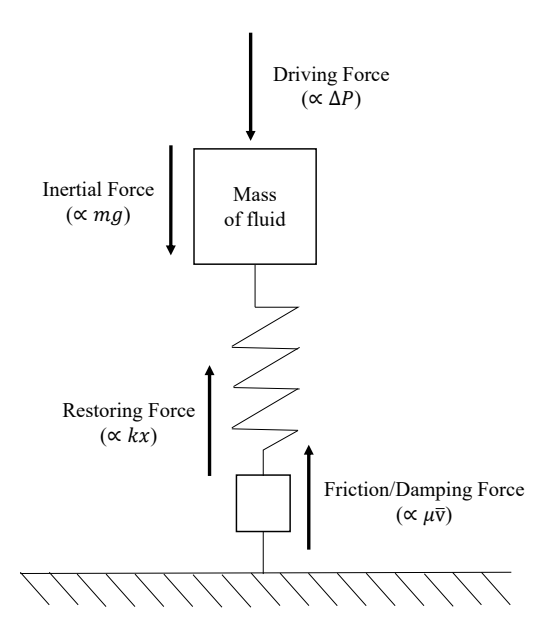


Fig. 5. Mechanical mass-spring model for liquid slug oscillation in PHP.

working fluid by comparing it to a standard spring mechanical system [14]. The gas spring constant can also be expressed as a function of $T_{\rm evap}$ using the equation for calculating the restoring force $F_{\rm R}$

$$F_{\rm R} = \kappa x = A_{\rm c} \Delta P_{\rm evap} = A_{\rm c} \frac{\rho_{\rm v} \Re T_{\rm evap}}{L_{\rm v}} x,$$
 (11)

where x is the position along the micro-channel, and $L_{\rm v}$ is the total length of the vapor bubbles in the micro-channels. When x is divided by both sides, κ becomes

$$\kappa = A_{\rm c} \frac{\rho_{\rm v} \Re T_{\rm evap}}{L_{\rm v}}.$$
 (12)

Since the evaporator temperature is linearly proportional to the gas spring constant, as $T_{\rm evap}$ increases, κ increases at the same rate.

Using the minimum and maximum κ values from Eq. 12, the slug oscillation frequency can be calculated as

$$\omega = \sqrt{\frac{\kappa}{m}},\tag{13}$$

where m is the total mass of the fluid in the microchannels. From Ma's [14] equation for calculating the damping coefficient

$$C^* = A_{\rm c} \left[(f_{\rm L} \cdot \text{Re}_{\rm L}) \left(\frac{\mu_{\rm L} L_{\rm L}}{2D^2} \right) + (f_{\rm v} \cdot \text{Re}_{\rm v}) \left(\frac{\mu_{\rm v} L_{\rm v}}{2D^2} \right) \right]$$
(14)

where f is the friction factor, Re is the Reynolds number, μ is the dynamic viscosity, and D_h is the hydraulic diameter of the channel. Since the flow operates under laminar conditions, the damping coefficient equation is

$$C^* = A_{\rm c} \left[64 \left(\frac{\mu_{\rm L} L_{\rm L}}{2D_h^2} \right) + 64 \left(\frac{\mu_{\rm v} L_{\rm v}}{2D_h^2} \right) \right]. \tag{15}$$

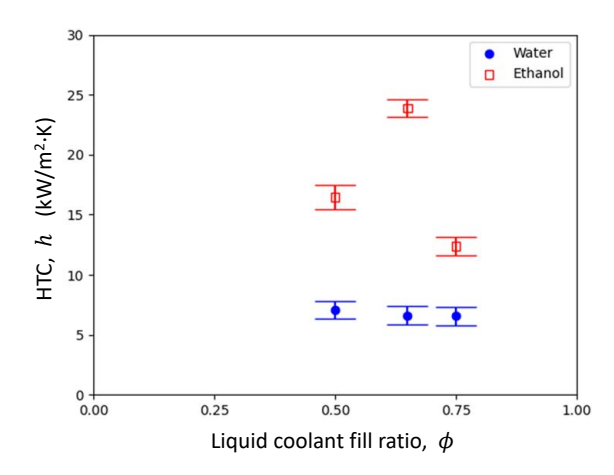


Fig. 6. Average heat transfer coefficient (HTC, h) as a function of fill ratio.

Using this coefficient, we can then calculate the damping ratio,

$$\zeta = \frac{C^*}{2m\omega}.\tag{16}$$

Based on Eqs. 12-16, the gas spring constant ranges within 0.6 μ N/m $\lesssim \kappa \lesssim 1.1 \ \mu$ N/m. The average oscillation frequency is $\omega_{\rm avg} \approx 0.158$ Hz and the average damping ratio is $\zeta_{\rm avg} \approx 47.7$.

III. RESULTS AND DISCUSSION

A. Heat Flux and HTC Values of PHP

Since water has a large surface tension and latent heat of vaporization, theoretically it should be superior to ethanol as a working fluid. In this work however, ethanol actually out performed water. Fig 6. shows the HTCs for both ethanol and water as a function of the liquid fill ratio (ϕ). The ethanol fluid was more sensitive to changes in fill ratio. We also note that the maximum heat flux data for sustained operation between the two fluids were similar. For example, water and ethanol both yielded sustained operational regimes at heat fluxes ranging within 3 W/cm² $\lesssim q \lesssim 8$ W/cm². This could be due to the differences in vapor density causing a change in vapor pressure, subsequently allowing for sustained pulsations with similar applied heat fluxes (heating powers).

From the maximum heat flux values, we can calculate the maximum heat transfer coefficient values using Eq. 4. For water and ethanol, the max HTC values, based on temperature data from the IR camera, were $\approx 11.5~\text{kW/m}^2 \cdot \text{K}$ and $\approx 26.7~\text{kW/m}^2 \cdot \text{K}$, respectively. Likewise, since water had a larger difference in temperature between the fluid and the evaporator compared to ethanol, its average HTC value was also <1/2 of that for ethanol's average HTC (Fig. 6). These results match with that observed by Mameli et al. [16], which had similar heat fluxes with ethanol at approximately ten times our input heater power. Although our average heat transfer coefficient is approximately three times their results. Also, the heat flux and HTC performance trends for both water and ethanol filled PHPs were nearly linear, which agrees with the

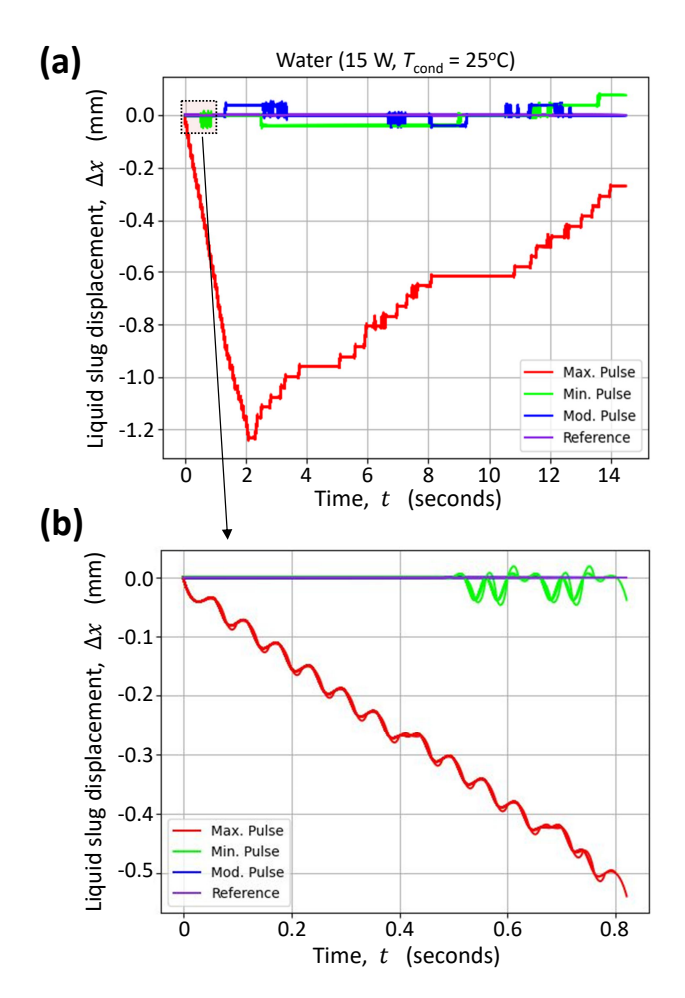


Fig. 7. Pulsation frequency data for ethanol ($\phi \approx 0.75$). (a) Pulsations data for three different slugs throughout the entire duration of the trial recording with a heater power setting of 15 W. (b) Zoom-view of data that shows the pulsations in the first second of the recording.

trends observed by Sonawane et al. [8] - specifically with ethanol as the PHP coolant.

B. Pulsation Frequency Measurements

Figures 7 and 8 provide data for the pulsation dynamics with water and ethanol filled PHPs, respectively. These results show that ethanol has a higher average net displacement and oscillation frequency compared to water. The results also show the dramatic spatiotemporal variations in the pulsation dynamics (especially if there is any change in the applied heater power). Figs. 7(b) and 8(b) highlight the differences in the pulsation dynamics between water and ethanol within 1 second after an increase in the applied (setpoint) heater power. For ethanol at t < 1 second the pulsations resemble that of a highly convoluted multimodal wave, whereas for water the pulsations resemble that of one high frequency sinewave modulated by one or more low frequency waves. Because our PHP configuration consists to two separated (top and bottom) condenser regions (rather than one single condenser region), the pulsation dynamics are better described by two coupled and nonlinearly damped gas springs. Therefore, modeling the

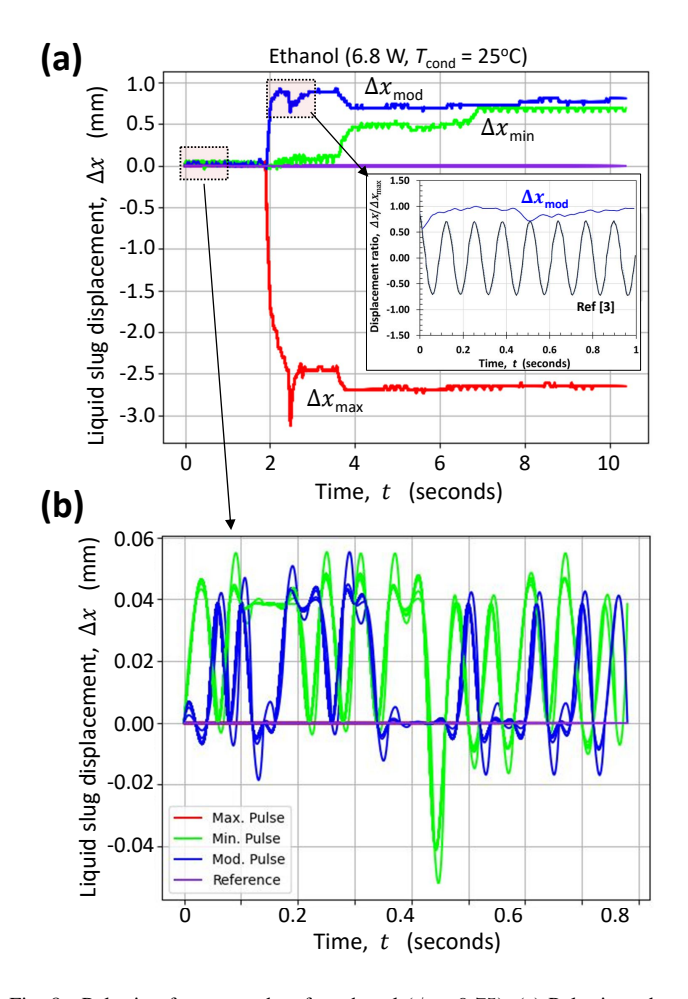


Fig. 8. Pulsation frequency data for ethanol ($\phi \approx 0.75$). (a) Pulsations data for three different slugs throughout the entire duration of the trial recording with a heater power setting of 6.8 W. (b) Zoom-view of data that shows the pulsations in the first second of the recording. The subset plot in (a) provides the normalized displacement ratio ($\Delta x/\Delta x_{\rm max}$) verses time, comparing that acquired in this work for moderate slug pulsations to that published in [3].

liquid (or vapor) slug position and pulsation amplitude as a function of time using the literature [2, 14] gas-spring PHP equations (Eqs. 5-16) was not feasible.

In this study, all tests were done vertically, where the gravitational forces affected the oscillations and thermal performance of the PHP. With the assistance of gravity for most fluids, the amount of heat the PHP is capable of absorbing increases and can reach its maximum capacity. As a PHP rotates from a horizontal position to a vertical position the thermal resistance tends to decrease which increases the heat transfer coefficient and the heat flux. With the help of gravity, the working fluid from the condenser to the heater contributes to the increase in pulsations and showed better performance in the transfer of heat [17].

IV. CONCLUSION

The use of flexible PHPs is projected to be a promising method for cooling flexible electronics. Based on the PHP results provided herein, the pulsations were more efficient for ethanol than for water, while the maximum heat fluxes obtained for both coolants were similar. However, the overall heat transfer coefficients and pulsation frequencies were notably different for ethanol and water, warranting further testing – especially a larger range liquid-to-vapor fill ratios. This study also explored the feasibility of using a simple gas spring model for predicting liquid slug oscillations (Figs. 7(b) and 8(b)). However, our results were highly influenced by gravity; therefore further studies in the horizontal configuration are needed for model validation.

Future studies will investigate stacked PHPs (i.e., 3D PHP architectures) at increased power loads [18]. Use of highly flexible materials with Young's moduli below that for human skin ($E < 100 \, \mathrm{kPa}$) are also of key interest. For example, PHPs fabricated from optical adhesives and silicone elastomers (i.e., Ecoflex) due to their rapid replica molding capabilities and potential use in devices requiring bend radii $< 5 \, \mathrm{mm}$.

V. ACKNOWLEDGMENTS

This material is based on research primarily sponsored by the National Science Foundation (Grant No. 1653396).

REFERENCES

- [1] K. Bao, X. Wang, Y. Fang, X. Ji, X. Han, and G. Chen, "Effects of the surfactant solution on the performance of the pulsating heat pipe," *Applied Thermal Engineering*, vol. 178, p. 115678, 2020.
- [2] M. B. Shafii, A. Faghri, and Y. Zhang, "Thermal modeling of unlooped and looped pulsating heat pipes," *Journal of Heat Transfer*, vol. 123, no. 6, pp. 1159–1172, 05 2001.
- [3] Z. Zuo, M. North, and K. Wert, "High heat flux heat pipe mechanism for cooling of electronics," *IEEE Transactions on Components and Packaging Technologies*, vol. 24, no. 2, pp. 220–225, 2001.
- [4] H. Akachi, R. Polasek, and P. Stulc, "Pulsating heat pipes," in *Proc. 5th International Heat Pipe Symposium, Melbourne, Australia*, 1996, pp. 208–217.
- [5] T. Arai and M. Kawaji, "Thermal performance and flow characteristics in additive manufactured polycarbonate pulsating heat pipes with novec 7000," *Applied Thermal Engineering*, vol. 197, p. 117273, 2021.
- [6] J. Jo, J. Kim, and S. J. Kim, "Experimental investigations of heat transfer mechanisms of a pulsating heat pipe," *Energy Conversion and Management*, vol. 181, pp. 331– 341, 2019.
- [7] J. Lim and S. J. Kim, "Fabrication and experimental evaluation of a polymer-based flexible pulsating heat pipe," *Energy Conversion and Management*, vol. 156, pp. 358–364, 2018.
- [8] C. R. Sonawane, K. Tolia, A. Pandey, A. Kulkarni, H. Punchal, K. K. Sadasivuni, A. Kumar, and M. Khalid, "Experimental and numerical analysis of heat transfer and fluid flow characteristics inside pulsating heat pipe," *Chemical Engineering Communications*, vol. 210, no. 4, pp. 549–565, 2023.

- [9] P. Charoensawan, S. Khandekar, M. Groll, and P. Terdtoon, "Closed loop pulsating heat pipes: Part a: parametric experimental investigations," *Applied Thermal Engineering*, vol. 23, no. 16, pp. 2009–2020, 2003.
- [10] M. L. Rahman, M. F. Kader, M. Z. Rahman, and M. Ali, "Experimental investigation on thermal performance of a closed loop pulsating heat pipe without fin and with fin structure," *American Journal of Mechanical Engineering*, vol. 4, no. 6, pp. 209–214, 2016.
- [11] X. M. Zhang, "Experimental study of a pulsating heat pipe using fc-72, ethanol, and water as working fluids," *Experimental Heat Transfer*, vol. 17, no. 1, pp. 47–67, 2004.
- [12] C. B. Tibiriçá, L. E. Czelusniak, and G. Ribatski, "Critical heat flux in a 0.38mm microchannel and actions for suppression of flow boiling instabilities," *Experimental Thermal and Fluid Science*, vol. 67, pp. 48–56, 2015, heat Transfer and Fluid Flow in Microscale.
- [13] B. Tong, T. Wong, and K. Ooi, "Closed-loop pulsating heat pipe," *Applied Thermal Engineering*, vol. 21, no. 18, pp. 1845–1862, 2001.
- [14] H. Ma, Oscillating Heat Pipes. New York: Springer, 2015.
- [15] T. Germain, C. Brewer, J. Scott, and S. A. Putnam, "Scalable stamp printing and fabrication of hemiwicking surfaces," *JoVE (Journal of Visualized Experiments)*, no. 142, p. e58546, 2018.
- [16] M. Mameli, M. Marengo, and S. Khandekar, "Flow patterns and corresponding local heat transfer coefficients in a pulsating heat pipe," in *Proceedings of the 29th National Heat Transfer Conference of Italy, Politecnico* di Torino, Torino, Italy, June 2011.
- [17] M. Xing, R. Wang, and J. Yu, "The impact of gravity on the performance of pulsating heat pipe using surfactant solution," *International Journal of Heat and Mass Transfer*, vol. 151, p. 119466, 2020.
- [18] O. T. Ibrahim, J. G. Monroe, S. M. Thompson, N. Shamsaei, H. Bilheux, A. Elwany, and L. Bian, "An investigation of a multi-layered oscillating heat pipe additively manufactured from ti-6al-4v powder," *International Journal of Heat and Mass Transfer*, vol. 108, pp. 1036–1047, 2017.